Freestanding Oxide Ferroelectric Tunnel Junction Memories Transferred onto Silicon

Di Lu,[*,†,∥] Sam Crossley,[‡] Ruijuan Xu,[‡,§] Yasuyuki Hikita,[§] and Harold Y. Hwang[*,‡,§]

[†]Department of Physics, Stanford University, Stanford, California 94305, United States

[‡]Department of Applied Physics, Stanford University, Stanford, California 94305, United States

[§]Stanford Institute for Materials and Energy Sciences, SLAC National Accelerator Laboratory, Menlo Park, California 94025, United States

ABSTRACT: Crystalline oxide ferroelectric tunnel junctions enable persistent encoding of information in electric polarization, featuring nondestructive readout and scalability that can exceed current commercial high-speed, nonvolatile ferroelectric memories. However, the well-established fabrication of epitaxial devices on oxide substrates is difficult to adapt to silicon substrates for integration into complementary metal-oxide-semiconductor electronics. In this work, we report ferroelectric tunnel junctions based on 2.8 nm-thick $BaTiO_3$ films grown epitaxially on $SrTiO_3$ growth substrates, released, and relaminated onto silicon. The performance of the transferred devices is comparable to devices characterized on the oxide substrate, suggesting a viable route toward next-generation nonvolatile memories broadly integrable with different materials platforms.

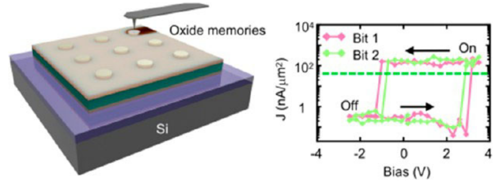

KEYWORDS: *Nonvolatile memories, freestanding, oxides, ferroelectric tunnel junctions, pick and place*

Ferroelectric memories allow high-speed, nonvolatile information storage by encoding '0' and '1' states into their switchable remnant polarizations. Given such advantages, the ferroelectric random access memory (FeRAM) was once expected to become a main form of commercial memory devices,[1] yet later faced substantial barriers such as low scalability and destructive readout (data require rewriting after reading) due to their capacitive readout process.[2] Recently, the development of another form of ferroelectric memory, oxide epitaxial ferroelectric tunnel junctions (FTJs), utilized a resistive reading process by measuring the tunnel current, which is strongly modulated by the ferroelectric polarization, under small (<1 V) DC bias. The large tunnel current density (>10 nA/μm^2) enabled by a small ferroelectric barrier thickness (1−4 nm) made nanometer-sized devices feasible, realizing data densities up to a few gigabit/cm^2. Furthermore, the readout process is nondestructive, given that the reading bias is far below the switching voltage (~2−5 V).[2,3]

Although featuring such superior properties, the single crystal oxide substrates the FTJs are typically grown on[4−9] are incompatible with current silicon-based fabrication processes (for example, it is difficult for oxide substrates to host Si complementary metal-oxide-semiconductor (CMOS) control circuits),[10] limiting many further applications of the FTJs. Direct deposition of FTJs on Si compromises the crystallinity, yielding larger devices with diminished characteristics.[11] Deposition of epitaxial FTJs on Si by inserting $SrTiO_3$ buffer layers has been demonstrated, yet factors critical for future applications, especially device uniformity, are not fully investigated.[12] Moreover, this approach suffers complexities arising to reduce the chemical reaction at the interface between the oxide and Si as well as to retain the epitaxial relationship.[12−16] Using high-power laser irradiation to lift epitaxial oxides from native substrates[17−19] then transfer to Si or transferring two-dimensional oxide nanosheets as an epitaxial growth template[20,21] on Si are other possible fabrication methods, although FTJs for these cases have not been reported. Here we demonstrate the transfer of epitaxial FTJs from oxide substrates to Si using released freestanding films, greatly simplifying the fabrication process. The metrics of transferred FTJ performance, including tunnel current density, switching voltage, and other specifications such as on−off ratio and stability (uniformity and repeatability), are comparable with epitaxial FTJs on oxide substrates reported here and in the literature, paving paths toward possible future nonvolatile memory applications.

Our approach to releasing FTJs from oxide substrates is to insert an epitaxial, water-soluble $Sr_3Al_2O_6$ layer between the device heterostructure and the oxide substrate, followed by selective etching of the sacrificial $Sr_3Al_2O_6$ (Figure 1a) as reported in ref 22. Previous work shows that this process is minimally disruptive to the lattice structure of the transferred layer, allowing us to maintain the high quality of the epitaxial FTJ stacks after transfer. Elemental metal/$BaTiO_3$/$La_{0.7}Sr_{0.3}MnO_3$ FTJs are widely studied, and their performance serves as a benchmark of the current FTJs.[3−7] For this purpose, we grew a $Sr_3Al_2O_6$ (8.8 nm) sacrificial layer and a $BaTiO_3$/

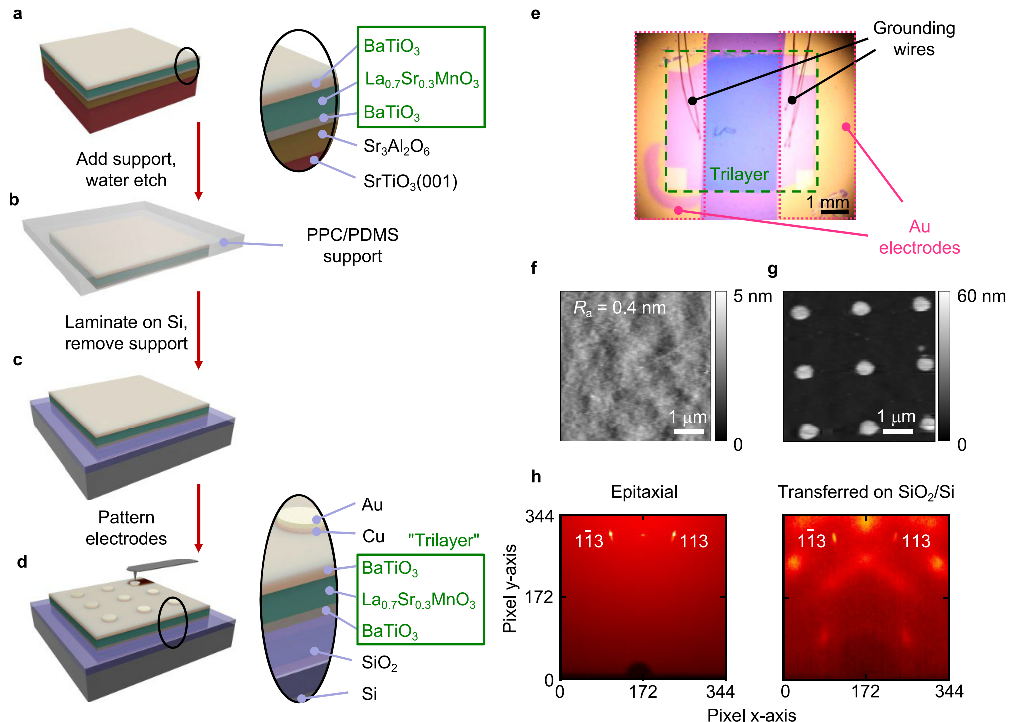

Figure 1. Fabrication and structural characterization of the FTJs transferred on SiO_2-coated Si substrates. (a−d) Schematics of (a) an epitaxial $BaTiO_3$ (2.8 nm)/$La_{0.7}Sr_{0.3}MnO_3$ (10 nm)/$BaTiO_3$ (2.8 nm)/$Sr_3Al_2O_6$ (8.8 nm)/$SrTiO_3$ (001) heterostructure; (b) a released $BaTiO_3$/$La_{0.7}Sr_{0.3}MnO_3$/$BaTiO_3$ trilayer attached to a PPC/PDMS supporting polymer; (c) a transferred trilayer on SiO_2/Si; and (d) a trilayer with deposited Au (30 nm)/Cu (30 nm) electrodes. (e) Optical image of a 5 × 5 mm^2 transferred trilayer (enclosed in the dashed line) with Au grounding electrodes on left and right for ohmic contacts of the $La_{0.7}Sr_{0.3}MnO_3$ layer (enclosed in the dotted line). Four pads at the corners of the transferred trilayer are markers. (f, g) Surface morphology of the transferred trilayer (f) without and (g) with the Au/Cu electrodes (500 nm diameter) measured by AFM. (h) GIXRD of an epitaxial trilayer and a transferred trilayer showing perovskite ($1\bar{1}3$) and (113) peaks and no Debye rings after transfer. The additional features observed in transferred trilayer GIXRD are from the SiO_2/Si substrate.

$La_{0.7}Sr_{0.3}MnO_3$/$BaTiO_3$ (2.8, 10 and 2.8 nm, respectively) trilayer[22−24] on a $SrTiO_3$(001) substrate by pulsed laser deposition (PLD, Figure 1a, see Supporting Information). The uppermost $BaTiO_3$ layer forms part of the FTJ device; the lower $BaTiO_3$ layer of equal thickness was designed to create a symmetrically strained membrane. Next, the top surface of the as-grown heterostructure was adhered on a polypropylene carbonate (PPC)/polydimethylsiloxane (PDMS) support and immersed in water, dissolving the $Sr_3Al_2O_6$ and allowing the growth substrate to be removed (Figure 1b). The released trilayer was then relaminated on an oxide-coated (SiO_2 300 nm) Si (001) substrate (Figure 1c). As the last step, arrays of circular Cu/Au electrodes (30/30 nm thick, 500 nm diameter) were fabricated on top, forming Cu-$BaTiO_3$-$La_{0.7}Sr_{0.3}MnO_3$ FTJs using e-beam lithography (Figure 1d).

Figure 1e presents an optical image of a transferred FTJ device trilayer on Si. Despite the large aspect ratio (5 mm × 5 mm × 16 nm), no physical cracks were observed on the heterostructure across the entire surface. The 5 kΩ in-plane resistance of the trilayer, measured by wire-bonding through two Au pads at two ends (Figure 1e), was in good agreement with the 10.8 kΩ (5.4 kΩ) resistance of a 10 nm-thick epitaxial (freestanding) $La_{0.7}Sr_{0.3}MnO_3$ layer,[22] suggesting no significant degradation of its electric properties during transfer. Atomic force microscopy (AFM) on uncoated and electrode-coated areas showed a smooth surface (arithmatic roughness $R_a \sim 0.4$ nm, Figure 1f) and densely packed electrode arrays (Figure 1g), respectively. The single crystallinity of the transferred trilayer was confirmed by grazing incidence X-ray diffraction (GIXRD), where the characteristic ($1\bar{1}3$) and (113) peaks of the perovskite oxides were well-preserved for the trilayer, and no Debye rings indicating polycrystallinity were observed (Figure 1h).

The ferroelectric properties of the uncoated $BaTiO_3$ in the transferred trilayer were probed by piezoresponse force microscopy (PFM) using a conductive AFM tip scanning across a 2 μm × 2 μm area. Tip-$La_{0.7}Sr_{0.3}MnO_3$ voltages of ±4 V were applied following concentric-square patterns. The out-of-plane PFM phase signal under contact resonance was subsequently mapped out in the absence of bias voltage (Figure 2a), revealing a phase contrast close to 180° between areas previously exposed to positive or negative bias. This strongly suggests the polarization of the $BaTiO_3$ layer was nearly vertically aligned and switchable by the applied voltage. Further switching tests by applying lateral stripe patterns with voltage of ±4 V on the same area controlled against the possibility of irreversible electrochemical reaction (Figure 2b).[25] We also did not observe relaxation behavior of the PFM phase map up to 30 min, which would be an indicator of reversible migration of oxygen vacancies.[25] To probe hysteresis, we fixed the tip position and gradually incremented and decremented the bias voltage between ±4 V in a sweep which was interspersed by measurements of the PFM signal in absence of any bias. The resulting hysteresis loop in phase and amplitude evidenced switching at a positive and negative coercive voltage V_{c+} = +2.7 V and V_{c-} = −1.9 V (Figure 2c), similar to the value reported for epitaxial $BaTiO_3$ (2.8 nm) thin films.[9] The small ∼0.8 V asymmetry is attributable to an

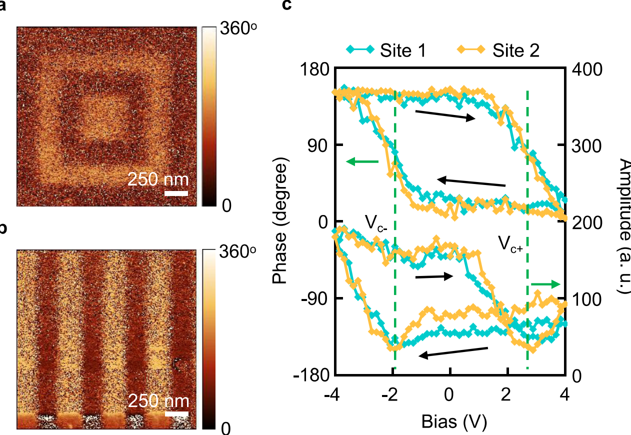

Figure 2. Ferroelectricity of the $BaTiO_3$ top layer in the transferred trilayer probed by PFM. (a, b) Out-of-plane PFM phase map after sequential biasing in (a) a concentric-square pattern and (b) a stripe pattern. (c) Out-of-plane PFM phase and amplitude at two random sites with gradually incremented and decremented bias voltage showing characteristic hysteresis. The dashed line indicates the positive and negative coersive voltages, V_{c+} and V_{c-}.

interfacial nonswitchable, electrode-dependent polarized layer imposed by asymmetric electrodes.[26] PFM mapping and hysteresis measurements on the as-grown epitaxial $BaTiO_3$/$La_{0.7}Sr_{0.3}MnO_3$/$BaTiO_3$/$Sr_3Al_2O_6$/$SrTiO_3$(001) yields similar reversible switching behavior and asymmetry of the coercive voltages, suggesting the ferroelectricity of the top $BaTiO_3$ layer is well preserved after transfer (Figure S1). Note that the incomplete 180° switching in the unreleased structure may be attributed to the stress generated by the AFM tip due to the different mechanical boundary conditions, including under partial absorption of atmospheric humidity in the sacrificial layer.[27]

To probe the resistive switching behaviors of our Cu/$BaTiO_3$/$La_{0.7}Sr_{0.3}MnO_3$ FTJs, a conductive AFM tip was used to make electrical contact to the Cu top electrodes, and bias voltages were applied to it with respect to the $La_{0.7}Sr_{0.3}MnO_3$ bottom electrode. Voltage pulses of amplitude ranging from −2.5 V to +3.5 V were applied across the FTJs and interspersed by measurements of the DC conductivity at a nominally nonperturbative bias of 0.2 V (Figure 3a). A >100-fold contrast in tunnel current between the low-resistance state (‘on’ state, ~200 nA/μm^2) and high-resistance state (‘off’ state, ~0.5 nA/μm^2) was observed, clearly distinguishing the binary logic value stored in the FTJ. The switching voltages of V_{s+} = +2.9 V and V_{s-} = −1.5 V agreed well with the ferroelectric coercive voltage V_{c+} = +2.7 V and V_{c-} = −1.9 V measured by PFM. The resistive switching behavior of 17 devices featured similar ‘on’ and ‘off’ currents that were all separated at ~50 nA/μm^2 (Figure 3b), showing high uniformity of our devices.

To examine the compatibility of our memory devices and the writing sequences generated by Si CMOS control circuits,[10] single voltage pulses at +3.5 V and −2.5 V were applied on an FTJ. 100 repeated switchings similarly yielded a ~50 nA/μm^2 separation (Figure 3c), demonstrating good repeatability. No significant decay of the resistive states was observed at least for 30 min (Figure 3d), suggesting long-term information retention, while ruling out the scenario of polarization loss due to the imperfect electrode−tunnel barrier interface causing inefficient depolarization field screening.[7]

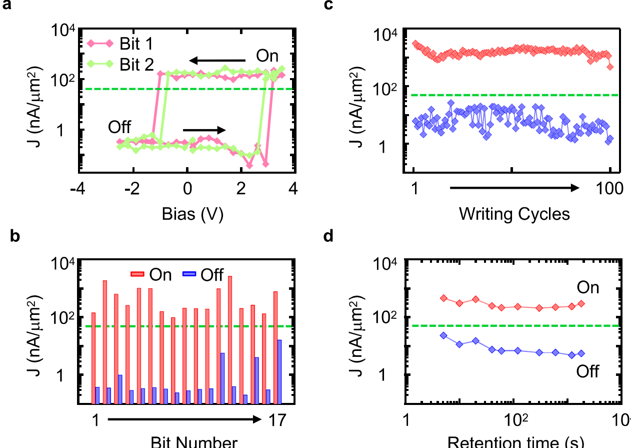

Figure 3. Resistive switching behavior of the transferred FTJs. (a) Tunnel current measured at 0.2 V DC voltage after a gradually incremented and decremented pulsed bias showing characteristic hysteresis loops for two different junctions. (b−d) On (red, low-resistance state, switched at +3.5 V) and off (blue, high-resistance state, switched at −2.5 V) currents of (b) 17 different tunnel junctions, (c) 100 subsequent switching for one tunnel junction, and (d) one tunnel junction after pausing for up to 30 min after switching to either ‘on’ or ‘off’ state. Green dashed line is the 50 nA/μm^2 line separating ‘on’ or ‘off’ states.

To confirm that our transfer process maintains the high quality of the FTJs fabricated on oxide substrates, we compare the parameters characterizing the performance of our devices with literature reported metal/$BaTiO_3$/$La_{0.7}Sr_{0.3}MnO_3$ devices (Figure 4).[4−8,12] Our current densities J of each state (200 nA/μm^2 for ‘on’, 0.5 nA/μm^2 for ‘off’) and switching voltages V_s of ~2 V per 2.8 nm of $BaTiO_3$ are similarly consistent with literature reports of epitaxial devices. Importantly, our ‘on’

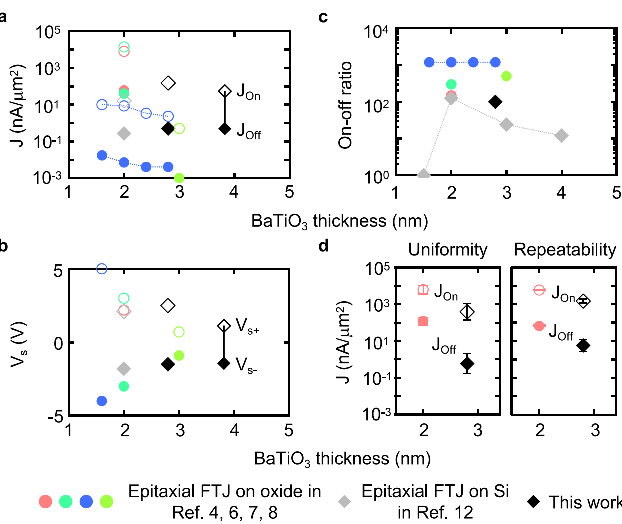

Figure 4. Comparison of the metrics between the transferred FTJs and reported epitaxial FTJs with elemental metal/$BaTiO_3$/$La_{0.7}Sr_{0.3}MnO_3$ structures. (a) ‘On’ (solid symbols) and ‘off’ (open symbols) tunnel current densities; (b) positive (solid symbols) and negative (open symbols) switching voltages; (c) on−off ratios; and (d) uniformity and repeatability by the standard variations (error bars) of ‘on’ (solid symbols) and ‘off’ (open symbols) current densities. The current densities in different reports are normalized to readout voltage 0.2 V.

state current density is larger than 10 nA/μm^2, a representative threshold below which further device downscaling to gigabit/cm^2 is impeded due to the reduced signal-to-noise ratio,[2] and our switching voltage V_s is well above the reading bias voltage of 0.2 V, enabling a nondestructive readout. Another core parameter is the on−off ratio, the ratio between the current density of the 'on' and the 'off' states, describing the ease of distinguishing '0' and '1' in individual bits. Our ~100 on−off ratio is highly comparable with the values reported for epitaxial FTJs. We also compare the uniformity and repeatability, quantified by the standard deviation of J for 'on' and 'off' states; those of our devices (around ±0.5 order of magnitude) are slightly higher, but still comparable to the epitaxial devices.

We further performed a control experiment whereupon FTJs were fabricated by depositing nominally identical Au/Cu upper electrodes on as-grown epitaxial $BaTiO_3/La_{0.7}Sr_{0.3}MnO_3/BaTiO_3/Sr_3Al_2O_6/SrTiO_3(001)$ and characterized in the same manner as the freestanding FTJs. The switching voltages, current densities, and on−off ratios were comparable across the transferred FTJs (Figure 3a,b) and as-grown FTJs (Figure S2), demonstrating that functional properties of the as-grown heterostructure are robust to the transfer process with high fidelity.

In summary, we have demonstrated a simple fabrication method for oxide FTJs on silicon substrates by using a freestanding film transfer 'pick and place' technique. A resistive readout with ~100 on−off ratio was consistently realized with all key figures of merit showing good agreement with literature reports of FTJs on single crystalline oxide substrates. Our work exemplifies a viable route to integrated and potentially ultrathin epitaxial oxide devices on a Si platform, which nonetheless benefit from the superior quality of epitaxial all-oxide growth. Furthermore, transfer substrates need not be limited to rigid materials such as Si and could include flexible polymers for integration into flexible electronics.[28]

AUTHOR INFORMATION

Corresponding Authors

*E-mail: diluacademic@gmail.com.

*E-mail: hyhwang@stanford.edu.

ORCID

Di Lu: 0000-0001-9806-6806

Ruijuan Xu: 0000-0001-5046-0599

Present Address

‖Center of Biointegrated Electronics, Northwestern University, Evanston, Illinois 60208, United States

Author Contributions

D.L. fabricated and transferred the oxide epitaxial FTJs on silicon substrates. D.L., R.X., and S.C. characterized the transferred FTJs. The manuscript was written through contributions of all authors, and all authors have given approval to the final version of the manuscript.

Notes

The authors declare no competing financial interest.

ACKNOWLEDGMENTS

The authors thank Dr. Andy Quindeau for helpful discussions. This work was supported by the Department of Energy, Office of Basic Energy Sciences, Division of Materials Sciences and Engineering, under contract DE-AC02-76SF00515 (synthesis) and the Gordon and Betty Moore Foundation's EPiQS Initiative through Grant GBMF4415 (device characterization). S.C. acknowledges partial support by the Air Force Office of Scientific Research (AFOSR) Hybrid Materials MURI under award no. FA9550-18-1-0480. R.X. acknowledges partial support from Stanford Geballe Laboratory for Advanced Materials (GLAM) Postdoctoral Fellowship program.

ABBREVIATIONS

CMOS, complementary metal-oxide-semiconductor; FeRAM, ferroelectric random access memory; FTJ, ferroelectric tunnel junction; PLD, pulsed laser deposition; PPC, polypropylene carbonate; PDMS, polydimethylsiloxane; AFM, atomic force microscopy; GIXRD, grazing incidence X-ray diffraction; R_a, arithmatic roughness; PFM, piezoresponse force microscopy; V_{c+} and V_{c-}, positive and negative coercive voltage; V_{s+} and V_{s-}, positive and negative switching voltage; J, tunnel current density

REFERENCES

(1) Scott, J. F.; Dearaujo, C. A. P. *Science* **1989**, *246*, 1400−1405.

(2) Garcia, V.; Fusil, S.; Bouzehouane, K.; Enouz-Vedrenne, S.; Mathur, N. D.; Barthelemy, A.; Bibes, M. *Nature* **2009**, *460*, 81.

(3) Garcia, V.; Bibes, M. *Nat. Commun.* **2014**, *5*, 4289.

(4) Chanthbouala, A.; Crassous, A.; Garcia, V.; Bouzehouane, K.; Fusil, S.; Moya, X.; Allibe, J.; Dlubak, B.; Grollier, J.; Xavier, S.; Deranlot, C.; Moshar, A.; Proksch, R.; Mathur, N. D.; Bibes, M.; Barthelemy, A. *Nat. Nanotechnol.* **2012**, *7*, 101.

(5) Gao, X. S.; Liu, J. M.; Au, K.; Dai, J. Y. *Appl. Phys. Lett.* **2012**, *101*, 142905.

(6) Chanthbouala, A.; Garcia, V.; Cherifi, R. O.; Bouzehouane, K.; Fusil, S.; Moya, X.; Xavier, S.; Yamada, H.; Deranlot, C.; Mathur, N. D.; Bibes, M.; Barthelemy, A.; Grollier, J. *Nat. Mater.* **2012**, *11*, 860.

(7) Kim, D. J.; Lu, H.; Ryu, S.; Bark, C. W.; Eom, C. B.; Tsymbal, E. Y.; Gruverman, A. *Nano Lett.* **2012**, *12*, 5697.

(8) Soni, R.; Petraru, A.; Meuffels, P.; Vavra, O.; Ziegler, M.; Kim, S. K.; Jeong, D. S.; Pertsev, N. A.; Kohlstedt, H. *Nat. Commun.* **2014**, *5*, 5414.

(9) Wen, Z.; Li, C.; Wu, D.; Li, A.; Ming, N. *Nat. Mater.* **2013**, *12*, 617.

(10) Wang, Z.; Zhao, W.; Kang, W.; Bouchenak-Khelladi, A.; Zhang, Y.; Zhang, Y.; Klein, J.-O.; Ravelosona, D.; Chappert, C. *J. Phys. D: Appl. Phys.* **2014**, *47*, 045001.

(11) Ambriz-Vargas, F.; Kolhatkar, G.; Broyer, M.; Hadj-Youssef, A.; Nouar, R.; Sarkissian, A.; Thomas, R.; Gomez-Yanez, C.; Gauthier, M. A.; Ruediger, A. *ACS Appl. Mater. Interfaces* **2017**, *9*, 13262−13268.

(12) Guo, R.; Wang, Z.; Zeng, S.; Han, K.; Huang, L.; Schlom, D. G.; Venkatesan, T.; Ariando; Chen, J. *Sci. Rep.* **2015**, *5*, 12576.

(13) McKee, R. A.; Walker, F. J.; Chisholm, M. F. *Phys. Rev. Lett.* **1998**, *81*, 3014−3017.

(14) Shutthanandan, V.; Thevuthasan, S.; Liang, Y.; Adams, E. M.; Yu, Z.; Droopad, R. *Appl. Phys. Lett.* **2002**, *80*, 1803−1805.

(15) Gu, X.; Lubyshev, D.; Batzel, J.; Fastenau, J. M.; Liu, W. K.; Pelzel, R.; Magana, J. F.; Ma, Q.; Wang, L. P.; Zhang, P.; Rao, V. R. *J. Vac. Sci. Technol. B* **2009**, *27*, 1195.

(16) Reiner, J. W.; Kolpak, A. M.; Segal, Y.; Garrity, K. F.; Ismail-Beigi, S.; Ahn, C. H.; Walker, F. *Adv. Mater.* **2010**, *22*, 2919.

(17) Comyn, T. P.; Chakraborty, T.; Miles, R. E.; Milne, S. J. *Appl. Phys. Lett.* **2008**, *93*, 052909.
(18) James, C.; Chakraborty, T.; Brown, A.; Comyn, T.; Dorey, R.; Harrington, J.; Laister, A. J.; Miles, R. E.; Puchmark, C.; Xu, B.; Xiong, W.; Zhang, Q.; Milne, S. J. *J. Mater. Sci.* **2009**, *44*, 5325−5331.
(19) Do, Y. H.; Kang, M. G.; Kim, J. S.; Kang, C. Y.; Yoon, S. J. *Sens. Actuators, A* **2012**, *184*, 124−127.
(20) Nijland, M.; Thomas, S.; Smithers, M. A.; Banerjee, N.; Blank, D. H. A.; Rijnders, G.; Xia, J.; Koster, G.; ten Elshof, J. E. *Adv. Funct. Mater.* **2015**, *25*, 5140−5148.
(21) Shibata, T.; Ebina, Y.; Ohnishi, T.; Takada, K.; Kogure, T.; Sasaki, T. *Cryst. Growth Des.* **2010**, *10*, 3787−3793.
(22) Lu, D.; Baek, D. J.; Hong, S. S.; Kourkoutis, L. F.; Hikita, Y.; Hwang, H. Y. *Nat. Mater.* **2016**, *15*, 1255−1260.
(23) Song, J. H.; Susaki, T.; Hwang, H. Y. *Adv. Mater.* **2008**, *20*, 2528−2532.
(24) Ohtomo, A.; Hwang, H. Y. *J. Appl. Phys.* **2007**, *102*, 083704.
(25) Kalinin, S. V.; Jesse, S.; Tselev, A.; Baddorf, A. P.; Balke, N. *ACS Nano* **2011**, *5*, 5683−5691.
(26) Sun, P.; Wu, Y.-Z.; Zhu, S.-H.; Cai, T.-Y.; Ju, S. *J. Appl. Phys.* **2013**, *113*, 174101.
(27) Gruverman, A.; Kholkin, A.; Kingon, A.; Tokumoto, H. *Appl. Phys. Lett.* **2001**, *78*, 2751−2753.
(28) Kim, D. H.; Ahn, J. H.; Choi, W. M.; Kim, H. S.; Kim, T. H.; Song, J. Z.; Huang, Y. G. Y.; Liu, Z. J.; Lu, C.; Rogers, J. A. *Science* **2008**, *320*, 507−511.